Infrared fixed point in SU(2) gauge theory with adjoint fermions

Thomas DeGrand

Department of Physics, University of Colorado, Boulder, CO 80309, USA

Yigal Shamir and Benjamin Svetitsky

Raymond and Beverly Sackler School of Physics and Astronomy, Tel Aviv University, 69978 Tel Aviv, Israel

We apply Schrödinger-functional techniques to the SU(2) lattice gauge theory with $N_f = 2$ flavors of fermions in the adjoint representation. Our use of hypercubic smearing enables us to work at stronger couplings than did previous studies, before encountering a critical point and a bulk phase boundary. Measurement of the running coupling constant gives evidence of an infrared fixed point g_* where $1/g_*^2 = 0.20(4)(3)$. At the fixed point, we find a mass anomalous dimension $\gamma_m(g_*) = 0.31(6)$.

PACS numbers: 11.15.Ha, 11.10.Hi, 12.60.Nz

I. INTRODUCTION

Recently, there has been an upsurge in interest in applying the techniques of lattice gauge theory to theories with different numbers of colors, different numbers of flavors, and fermionic representations other than the fundamental [1–5]. The immediate phenomenological application of these studies is to candidate theories of physics beyond the Standard Model, in which new gauge dynamics allow the replacement of the fundamental Higgs boson by a bound state of new fermionic degrees of freedom—so-called "technicolor" theories [6]. More generally, it is an interesting question in quantum field theory: How do systems of gauge fields coupled to fermions behave?

Many studies attempt to characterize the behavior of a theory by computing a suitably defined running coupling constant. Perturbation theory [7, 8] gives us a first approach and a menu of possibilities to be confronted by numerical studies. The two-loop beta function is

$$\beta(g^2) = \frac{dg^2}{d\log\mu^2} = -\frac{b_1}{16\pi^2}g^4 - \frac{b_2}{(16\pi^2)^2}g^6, \qquad (1)$$

where, for an SU(N) gauge theory with N_f flavors of fermions in representation R,

$$b_1 = \frac{11}{3}C_2(G) - \frac{4}{3}N_f T(R), \qquad (2)$$

$$b_2 = \frac{34}{3}[C_2(G)]^2 - N_f T(R)\left[\frac{20}{3}C_2(G) + 4C_2(R)\right] \qquad (3)$$

Here $C_2(R)$ is the value of the quadratic Casimir operator in representation R [where G denotes the adjoint representation, so $C_2(G) = N$], while $T(R)$ is the conventional trace normalization. Three possibilities for the behavior of the massless theory are:

- triviality, $b_1 < 0$ in our conventions.
- QCD-like physics, $\beta(g^2) < 0$ for all g^2, meaning $b_1, b_2 > 0$ in Eq. (1). This is presumed to be associated with confinement and chiral symmetry breaking, as in ordinary QCD.
- a fixed point at $g = g_*$, such that $\beta(g_*^2) = 0$. For $b_1 > 0$ this comes about if $b_2 < 0$ and then g_* is an infrared-attractive fixed point (IRFP). Correlation functions decay algebraically at large distance, and there is no confinement, no chiral symmetry breaking, and indeed no particle spectrum. For a given representation R, the domain of (N_c, N_f) where an IRFP exists is called the "conformal window."

Technicolor demands a theory with QCD-like physics. *Walking* technicolor requires a QCD-like theory just outside the conformal window.

In a massive theory, the running coupling $g(\mu)$ is augmented by the running fermion mass $m(\mu)$. In addition to the beta function, one considers the anomalous dimension γ_m of the mass operator $\bar\psi\psi$. It determines the running of the mass parameter according to

$$\mu\frac{dm(\mu)}{d\mu} = -\gamma_m(g^2)m(\mu). \qquad (4)$$

In lowest order in perturbation theory,

$$\gamma_m = \frac{6C_2(R)}{16\pi^2}g^2. \qquad (5)$$

In the massless theories used for technicolor, γ_m governs the running of the condensate $\langle\bar\psi\psi\rangle$. It is thus an important diagnostic for realistic "extended" technicolor models, especially those based on walking. Phenomenological constraints on such models require it to have a large, nonperturbative value. If the massless theory is conformal, on the other hand, then near $m_q = 0$ the correlation length ξ scales as

$$\xi \sim m_q^{-1/y_m} \qquad (6)$$

where $y_m = 1 + \gamma_m(g_*)$ is the leading relevant exponent of the system [9, 10]. (Here m_q is the mass defined by the axial Ward identity—see below.)

Perturbation theory cannot make reliable predictions for properties of systems that evolve to become strongly

interacting at long distances. To address questions such as "where is the conformal window" and "what is the spectrum" (for a confining theory) or "what are the critical exponents" (for a conformal theory) requires nonperturbative methods. For us, this methodology is simulation of the lattice-regulated theory.

We present here a study of the SU(2) gauge theory coupled to two flavors of Dirac fermions in the adjoint representation of the gauge group. Following the introduction of this theory as a technicolor candidate [11, 12], several groups have performed numerical simulations [13–23]. Studies of the lattice theory's phase diagram [15, 16] and spectrum [13–16, 18, 19, 21] indicate that its weak-coupling phase is quite different from that of SU(2) or SU(3) gauge theories coupled to a small number of fundamental-representation fermions. Applications of the Schrödinger functional (SF) method [17, 20] and Monte Carlo renormalization group (MCRG) [23] have indicated that this theory has an IRFP. The reliability of this prediction is limited, however, by the lattice discretization used. The phase diagram obtained shows a first-order transition in strong coupling which terminates rather close to the claimed location of the IRFP. One consequence is that the value of g_*, if it exists, is poorly determined.

The main goal of our work was to determine whether this theory has an infrared fixed point. We have calculated the beta function for the SF coupling g^2 by carrying out simulations on a number of different lattice volumes. We are able to present strong, even definite evidence for an IRFP. The strength of our calculation comes from adoption of an improved fermion action that incorporates normalized hypercubic smearing, "nHYP fat links" [24, 25]. The fat-link action has been shown to effect a dramatic reduction of lattice artifacts when used for QCD simulations. As we found for the SU(3) theory with sextet fermions [26], this action moves the end point of the first order transition farther into strong coupling and allows us to examine a much larger range of the SF coupling without encountering it. The work of Hietanen *et al.* [17] was limited to the range $1/g^2 > 0.22$ while the estimate for g_*^2 was in the range 2.0 to 3.2 or $1/g_*^2 = 0.3$ to 0.5. We reach $1/g^2 \simeq 0.07$ to 0.10, depending on the volume, at the strongest bare coupling. (Here the beta function has changed sign, so the largest running coupling is obtained on the smallest volume.) We observe directly an IRFP at $1/g_*^2 = 0.20(4)(3)$ where the first error is statistical and the second is systematic. This is a slightly weaker coupling than the two-loop perturbative value of $g_*^2 = 7.9$ or $1/g_*^2 = 0.126$. With this result, we determine the value of the mass anomalous dimension at the IRFP, $\gamma_m(g_*) = 0.31(6)$; here the bulk of the error reflects the uncertainty in g_*.

The outline of the paper is as follows: In Sec. II we review our lattice action and the techniques we use to measure the beta function and γ_m. In Sec. III we present the phase diagram of the lattice theory. Sections IV and V contain our results for the running coupling constant and mass anomalous dimension. We discuss our results in the context of the literature in Sec. VI.

II. METHOD

The lattice calculations in our SU(2) study, following the Schrödinger functional method, were carried out in the same way as in our recent study of the SU(3) gauge theory with sextet fermions. We refer the reader to Ref. [26] for a detailed presentation. In Secs. II A and II B we give a short recapitulation to make this paper self-contained. In Sec. II C we describe at some length the extraction of the beta function from fits to the running coupling. The method used here is special to a theory with a slowly running coupling. Our method for calculating γ_m, again similar to that in our SU(3) work, is presented in Sec. II D.

A. Lattice action and simulation

We study the SU(2) gauge theory coupled to two flavors of dynamical fermions in the adjoint representation of the color gauge group. The lattice action is given by the single-plaquette gauge action and the Wilson fermion action with added clover term [27]. The gauge connections in the fermion action employ the differentiable hypercubic smeared link of Ref. [24], from which the adjoint-representation gauge connection for the fermion operator is constructed. [The adaptation of the original SU(3) construction to SU(2) is trivial.] The smearing parameters for the links are the same as in Ref. [24]: $\alpha_1 = 0.75$, $\alpha_2 = 0.6$, $\alpha_3 = 0.3$. The parameters that are inputs to the simulation are the bare gauge coupling $\beta = 4/g_0^2$ and the fermion hopping parameter κ, related to the bare mass m_0 by $\kappa = (8 + 2m_0)^{-1}$. Tests of nonperturbative improvement [28–30] indicate that we can safely set the clover coefficient to its tree-level value of unity.

The molecular dynamics integration is accelerated with an additional heavy pseudo-fermion field as suggested by Hasenbusch [31], multiple time scales [32], and a second-order Omelyan integrator [33]. Lattice sizes range from 6^4 to 16^4 sites.

We study the massless theory by fixing $\kappa = \kappa_c(\beta)$, the point at which the quark mass m_q vanishes for each β. We define m_q using the unimproved axial Ward identity (AWI),

$$\partial_t \sum_{\mathbf{x}} \langle A_0^a(\mathbf{x}, t)\mathcal{O}^a\rangle = 2m_q \sum_{\mathbf{x}} \langle P^a(\mathbf{x}, t)\mathcal{O}^a\rangle \,. \qquad (7)$$

where the axial current $A_\mu^a = \bar\psi\gamma_\mu\gamma_5(\tau^a/2)\psi$, the pseudoscalar density $P^a = \bar\psi\gamma_5(\tau^a/2)\psi$, and $\mathcal{O}^a$ could be any source. We follow the usual SF procedure and take the source to be the gauge-invariant wall source at $t = a$ as in Eq. (19) below. The correlation functions in Eq. (7)

are then measured at $t = L/2$, the midpoint of the lattice. The derivative is taken as the symmetric difference, $\partial_\mu f(x) = [f(x+\hat{\mu}a) - f(x-\hat{\mu}a)]/(2a)$.

On a finite lattice, the quark mass m_q generally depends on the lattice size L as well as on (β, κ). As we show below, the dependence on L is quite weak except at the strongest couplings. We generally defined κ_c by demanding $m_q = 0$ on a 12^4 lattice. Since the L dependence becomes significant at strong coupling (see the Appendix), we also carried out a complete SF calculation at a shifted κ for $\beta = 1.4$. As will be seen below, the results turned out to be insensitive to this shift.

B. Schrödinger functional and the running coupling

The Schrödinger functional (SF) [34–38] is an implementation of the background field method that is especially suited for lattice calculations. It involves performing simulations in a finite volume of linear dimension L, while imposing fixed boundary conditions on the gauge field. The classical field that minimizes the Yang–Mills action subject to these boundary conditions is a background color-electric field. By construction the only distance scale that characterizes the background field is L, so the n-loop effective action $\Gamma \equiv -\log Z$ gives the running coupling via

$$\Gamma = g(L)^{-2} S_{\rm YM}^{\rm cl}, \tag{8}$$

where $S_{\rm YM}^{\rm cl}$ is the classical action of the background field. When Γ is calculated non-perturbatively, Eq. (8) gives a non-perturbative definition of the running coupling at scale L. In a simulation, the coupling constant is determined through the differentiation of Eq. (8) with respect to some parameter η in the boundary conditions. This is an observable quantity,

$$\begin{aligned} \left.\frac{\partial \Gamma}{\partial \eta}\right|_{\eta=0} &= \left\langle \frac{\partial S_{YM}}{\partial \eta} - \mathrm{tr}\left(\frac{1}{D_F^\dagger} \frac{\partial (D_F^\dagger D_F)}{\partial \eta} \frac{1}{D_F} \right) \right\rangle \Bigg|_{\eta=0} \\ &= \frac{K}{g^2(L)}. \end{aligned} \tag{9}$$

The quantity K is just a number [35]. With boundary fields as described in Ref. [37], it takes the value $K = -12\pi$ in the infinite-volume limit; we use this value for finite volume as well, since the corrections are numerically small. We also impose twisted spatial boundary conditions on the fermion fields, following Ref. [36], $\psi(x+L) = \exp(i\theta)\psi(x)$, with $\theta = \pi/5$ on all three axes [38].

The observable (9) is quite noisy and requires long simulation runs, as shown in Table I.

TABLE I: Summary of simulation runs for obtaining the Schrödinger functional coupling g^2 at the bare couplings (β, κ_c), for the lattice sizes L used in this study. Trajectories were of unit length.

β	κ_c	trajectories			
		$L = 6a$	$L = 8a$	$L = 12a$	$L = 16a$
3.0	0.12682	16.2K	32.2K	30K	19.5K
2.5	0.1276	16.2K	32.2K	40.6K	27.2K
2.453	0.12766	16.2K	–	16.2K	–
2.445	0.12769	16.2K	16.2K	–	–
2.0	0.12967	16.2K	32.2K	41.6K	27.2K
1.985	0.12279	16.2K	–	16.2K	–
1.97	0.12991	16.2K	16.2K	–	–
1.75	0.13216	16.2K	32.2K	32.3K	41.8K
1.5	0.13617	16.2K	32.2K	46.2K	32.3K
1.4	0.13824	16.2K	32.2K	43K	33.2K

C. Extraction of the beta function

By calculating the inverse running coupling on lattices of size L and sL, we obtain the discrete beta function (DBF)

$$B(u,s) = \frac{1}{g^2(sL)} - \frac{1}{g^2(L)}, \qquad u \equiv \frac{1}{g^2(L)}\ . \tag{10}$$

The usual beta function refers to infinitesimal scale changes. We define the beta function for the inverse coupling as

$$\tilde{\beta}(1/g^2) \equiv \frac{d(1/g^2)}{d\log L} = 2\beta(g^2)/g^4 = 2u^2\beta(1/u). \tag{11}$$

Hence,

$$\log s = \int_L^{sL} \frac{dL'}{L'} = \int_u^{u+B(u,s)} \frac{du'}{\tilde{\beta}(u')}\ . \tag{12}$$

While the literature is careful to distinguish between the DBF and the usual beta function, we remark that in our theory the DBF's we can measure are, to high accuracy, just proportional to the beta function itself. This occurs for two reasons. First, our coupling runs slowly: We are, after all, near the (anticipated) bottom of the conformal window. Second, due to the cost of simulations, monitoring the volume dependence of the running coupling at fixed bare parameters is practical only for $s \lesssim 2$.

If the beta function changes little in the course of integrating Eq. (12), then the *rescaled* DBF, defined as

$$R(u,s) = \frac{B(u,s)}{\log s}\ , \tag{13}$$

will be approximately equal to the beta function $\tilde{\beta}(u)$. At one-loop order $R^{(1)}(u,s) = -2b_1/16\pi^2$, a constant

[compare Eqs. (1) and (11)]. The situation at the next order is illustrated in Fig. 1. The figure shows the two-loop result,

$$R^{(2)}(u,s) = -\frac{2b_1}{16\pi^2} - \frac{b_2}{16\pi^2 b_1} \times \frac{\log\left[1+(2b_1/16\pi^2)u^{-1}\log s\right]}{\log s}\ , \quad (14)$$

for the rescaled DBF for scale factor $s = 2$, 4, 8, compared to the one-loop and two-loop beta functions.[1] The rescaled DBF for $s = 2$ is hardly distinguishable from the beta function.

There are two lessons to be drawn from Fig. 1. If the actual DBF resembles the two-loop result, we can combine the rescaled DBF's for many scale factors s onto a single plot to give a good approximation to the actual beta function. Furthermore, since any value of $s \lesssim 2$ is as good as another, we can combine the couplings for all lattice volumes studied to extract the beta function via a fit.

We do not have to rely on perturbation theory when going beyond the approximation of a constant rescaled DBF. Expand the beta function $\tilde{\beta}(u)$ linearly near some fiducial value u_1,

$$\frac{du}{d\log s} = \tilde{\beta}(u_1) + (u-u_1)\tilde{\beta}'(u_1) = B_0 + B_1 u. \quad (15)$$

Upon integration,

$$u(s) - u_1 = \tilde{\beta}(u_1)\frac{\exp(B_1\log s) - 1}{B_1}\ . \quad (16)$$

When the product $B_1 \log s$ is small the exponential can be expanded, and we again observe that $[u(s)-u_1]/\log s = R(u,s)$ gives the beta function.

This discussion suggests that we can fit the running coupling from all volumes at fixed bare coupling to

$$1/g^2(sL_0) = c_0 + c_1\log s + c_2(\log s)^2 + \cdots\ , \quad (17)$$

where L_0 is a fixed reference volume. We treat all the parameters $c_0, c_1, c_2, \cdots$, as independent, having in mind that Eq. (15) is in itself just an approximation. If the terms nonlinear in $\log s$ are small, the slope c_1 gives the reduced DBF directly, according to Eq. (13). We do this below. The success of this analysis shows again that the beta function in this theory is small in the region studied; we use other fits to estimate the systematic error.

The discussion so far has ignored discretization errors. The usual analysis found in the literature presents the beta function only after an extrapolation to $(a/L) \to 0$. This is done by collecting data for DBF's on different volumes, and at the same value of g^2. We can do this by performing simulations at one value of the bare coupling β on our largest lattices (16^4 volumes), then moving to smaller volumes, matching $1/g^2(L)$ at fiducial volumes and measuring $1/g^2(sL)$ on appropriate larger volumes. For example, with $s = 2$ we can look at $L = 16$ and 8 at $\beta = 2.5$ (for example) compared to $L = 12$ and 6 at slightly offset β values. We must move along the κ_c line as we do this. We have attempted this at two values of the SF coupling. We found (see below) that the shifts in β were not well determined with the statistics available. This is, in fact, a disadvantage of having such a small beta function.

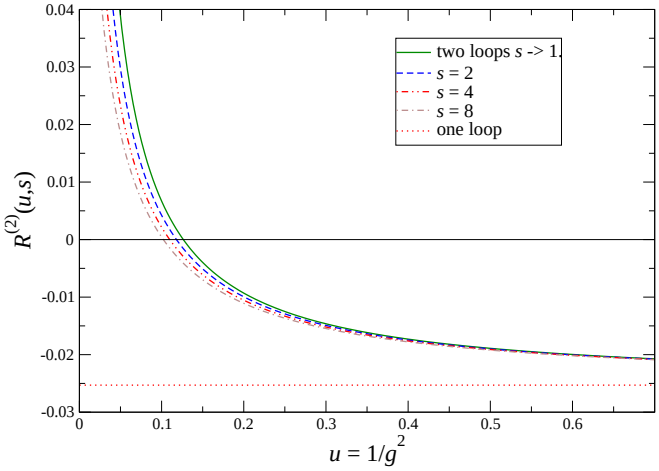

FIG. 1: Rescaled discrete beta function, calculated in two loops for various scaling factors s. Also shown are the one- and two-loop beta functions; the rescaled DBF approaches the two-loop beta function when $s \to 1$. Top to bottom, the curves are in the order shown in the legend.

Such an analysis, however, is needlessly complicated for the question we set out to answer, namely, is there an IRFP, and, if so, where is it? We can test various hypotheses for the dependence of the running coupling on the lattice volume at any fixed bare coupling. Equation (17) assumes that this dependence reflects continuum physics only; in addition, we will try fit functions that test if the volume dependence can be explained by the anticipated form of discretization errors, *i.e.*, powers of a/L. We can also test for the presence of lattice artifacts by varying the data sets kept in the fit. If the results agree on the existence and location of a zero of the DBF, then we can claim to have found an IRFP.

D. Mass anomalous dimension

The volume dependence of the renormalization factor Z_P of the isovector pseudoscalar density $P^a = \bar{\psi}\gamma_5(\tau^a/2)\psi$ gives the mass anomalous dimension γ_m. (The pseudoscalar density is related by a chiral rotation to $\bar{\psi}\psi$, which is the object of interest.) It is computed

[1] In this model, $b_1 = 2$ and $b_2 = -40$.

from two correlators via [20, 39–41]

$$Z_P = \frac{c\sqrt{f_1}}{f_P(L/2)}. \tag{18}$$

f_P is the propagator from the $t = 0$ boundary to a point pseudoscalar operator at time x_0,

$$f_P(x_0) = -\frac{1}{3}\sum_a \int d^3y\, d^3z \left\langle \overline{\psi}(x_0)\gamma_5 \frac{\tau^a}{2}\psi(x_0) \times \overline{\zeta}(y)\gamma_5 \frac{\tau^a}{2}\zeta(z)\right\rangle. \tag{19}$$

We take $x_0 = L/2$. In the expression, ζ and $\bar{\zeta}$ are gauge-invariant wall sources at $t = a$, i. e., one lattice layer away from the $t = 0$ boundary. The f_1 factor is the boundary-to-boundary correlator, which cancels the normalization of the wall source. Explicitly, it is

$$f_1 = -\frac{1}{3L^6}\sum_a \int d^3u\, d^3v\, d^3y\, d^3z \left\langle \overline{\zeta}'(u)\gamma_5 \frac{\tau^a}{2}\zeta'(v) \times \overline{\zeta}(y)\gamma_5 \frac{\tau^a}{2}\zeta(z)\right\rangle, \tag{20}$$

where ζ' and $\bar{\zeta}'$ are wall sources at $t = L - a$.

We use the same boundary conditions for the calculation of Z_P as for the simulations that generate the data for the SF coupling. This makes its computation parasitic on the SF runs.

The constant c allows imposing a volume-independent normalization condition in the weak-coupling limit. Since we will only need ratios of values of Z_P to find γ_m, the overall normalization is irrelevant. We set $c = 1/\sqrt{2}$ in tabulating Z_P below.

We extract the anomalous dimension of $\bar{\psi}\psi$ from the change in Z_P [Eq. (18)] between systems rescaled as $L \to sL$. The (continuum) mass step scaling function [20, 39–41] is

$$\sigma_P(v, s) = \left.\frac{Z_P(sL)}{Z_P(L)}\right|_{g^2(L)=v}. \tag{21}$$

It is related to the mass anomalous dimension via

$$\sigma_P(v, s) = \exp\left[-\int_1^s \frac{dt}{t}\,\gamma_m\left(g^2(tL)\right)\right]. \tag{22}$$

Because the SF coupling $g^2(L)$ runs so slowly, Eq. (22) is well approximated by

$$\sigma_P(g^2, s) = s^{-\gamma_m(g^2)}. \tag{23}$$

We can therefore combine many sL values collected at the same bare parameter values into one fit function giving γ_m,

$$\log Z_P(L) = -\gamma_m \log L + \text{const.} \tag{24}$$

This fitting procedure parallels keeping only the c_0 and c_1 terms in Eq. (17). As in the case of the DBF, we can look for subleading continuum corrections and/or for lattice artifacts by modifying the fit functions or the data set kept in the fit.

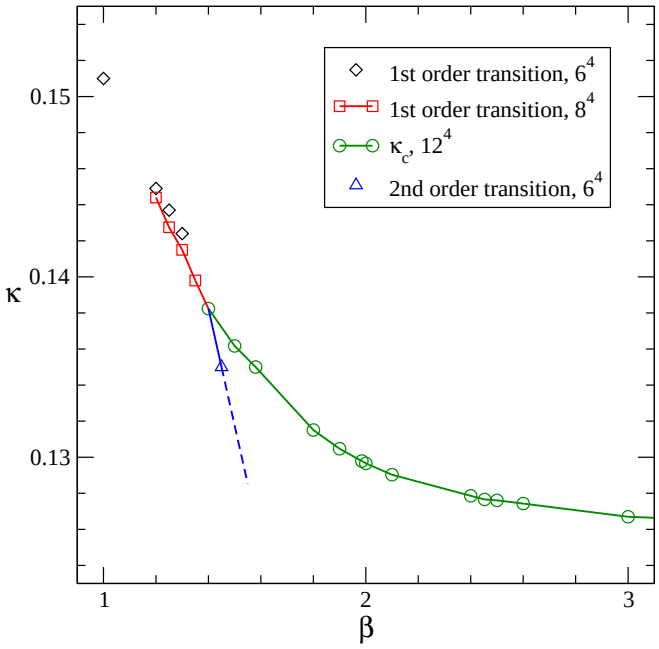

FIG. 2: Phase diagram in the β–κ plane, determined with Schrödinger functional boundary conditions. The κ_c line ends at a point (β^*, κ^*) presumed to be a critical point, where the indicated first-order boundary ends as well. The triangle marks a point on the second-order phase boundary between confined and deconfined phases. This phase boundary is presumed to continue all the way to $\kappa = 0$. Its upper endpoint may coincide with (β^*, κ^*).

III. PHASE DIAGRAM

Our determination of the phase diagram in the (β, κ) plane is preliminary. The diagram is qualitatively consistent with that given in Refs. [15, 16], but of course it is quantitatively different because of the fat-link action.

In order to measure the SF coupling, we had to map out the κ_c line. As discussed above, we determine κ_c by demanding $m_q = 0$ at fixed β; this is possible only for sufficiently weak coupling (large β—see Fig. 2). The κ_c line meets at $\beta = \beta^*$ a line of first order transition at which the AWI quark mass jumps discontinuously from a positive to a negative value; this makes it impossible to define κ_c for $\beta < \beta^*$. On the first-order line, the discontinuity in m_q, like that in the plaquette, varies with β and appears to vanish at β^* (see Fig. 3); this makes the meeting of the two lines a critical point. This is similar to what was reported in Refs. [15, 16].

In finite volume, another line of transitions separating the strong-coupling confining phase from a deconfined phase begins at or near the meeting point and runs out towards $\kappa = 0$. If the spatial volume were to be made large, this would be the finite-temperature confinement transition. The adjoint fermions leave the global Z(2) center symmetry unbroken, so the finite-temperature transition can be an Ising-like second order

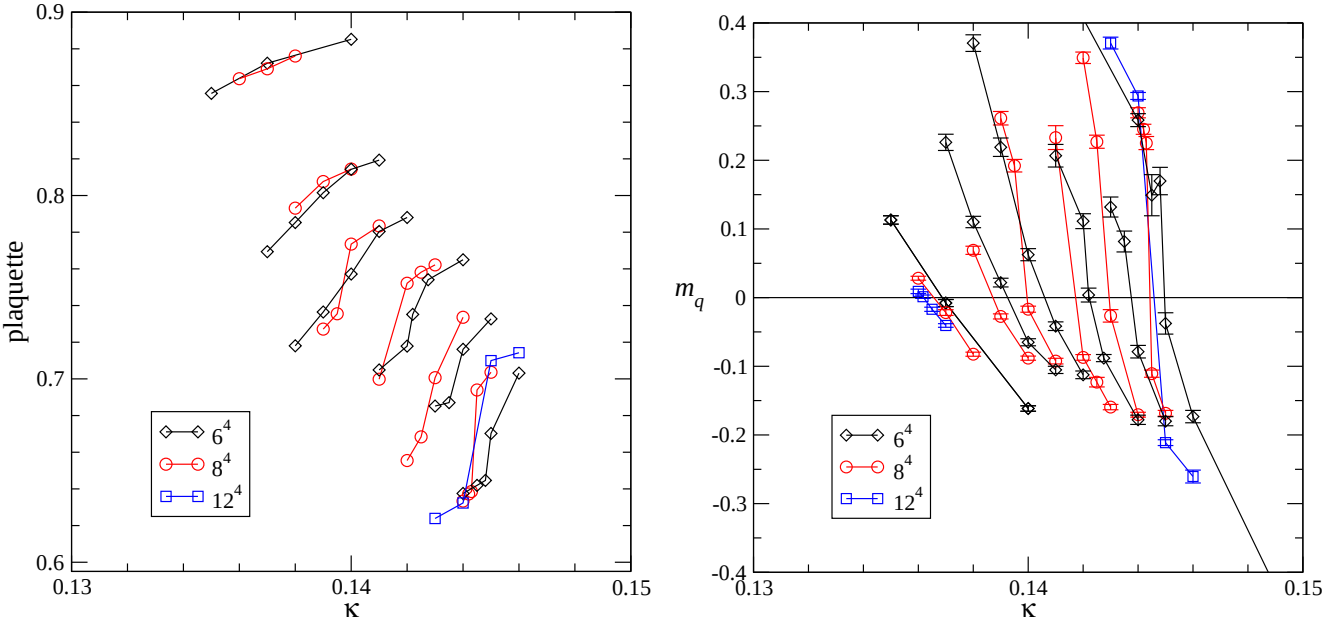

FIG. 3: Fixed-β scans of the average plaquette (left) and the AWI mass (right) on three different volumes. From right to left, the successive groups are for $\beta = 1.2$, 1.25, 1.3, 1.35, 1.4, and 1.5. For $\beta \leq 1.35$ there is a transition that strengthens with increased volume.

transition like that of the pure gauge theory. We have investigated this transition at one value of κ below the critical point and found it to be a continuous transition for volume 6^4 (Fig. 4), quite different from the jumps seen in the fixed-β scans of Fig. 3. The simplest scenario is to suppose a second-order phase boundary that stretches from $\kappa = 0$ to the critical point at (β^*, κ^*).

IV. RUNNING GAUGE COUPLING

Our SF calculations were performed along the κ_c line. A summary of the data collected is shown in Table I. The measured SF couplings are tabulated in Table II and plotted (for some values of β) in Fig. 5. The logarithmic variation of $1/g^2$ with L is characteristic of a slowly-running coupling. The transition from positive to negative slope as the bare coupling β decreases is our first piece of evidence for the existence of an IRFP.

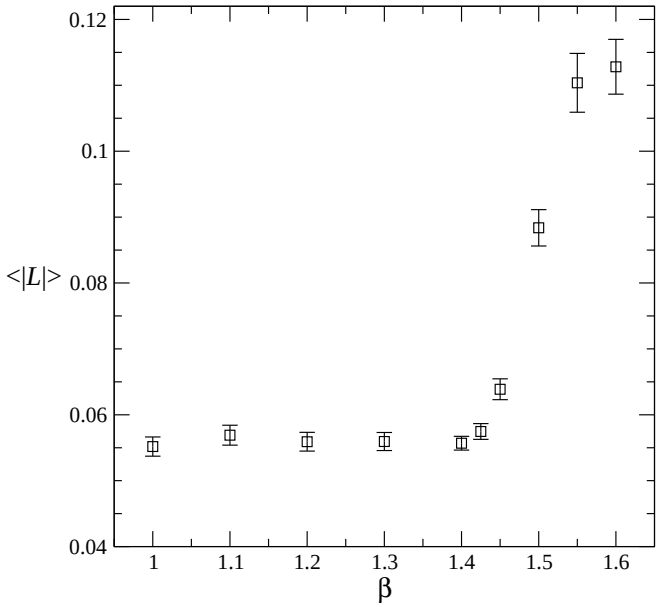

FIG. 4: Scan of the Polyakov loop average $\langle|L|\rangle$ at $\kappa = 0.135$ on volume 6^4.

A. The DBF for $s = 2$

The data can be combined in various ways. The most direct is to plot the $s = 2$ DBF for each of two values of L/a, 6 and 8. This is shown in Fig. 6; it is essentially a comparison of the DBF between two lattice spacings. The data for $L/a = 6$ and 8 give a picture of the DBF with only weak dependence on the lattice spacing. Remarkably, the numerical result tracks the two-loop DBF rather closely. We will estimate g_*, the location of the zero, in our more extensive analysis below.

At $\beta = 1.4$ we found that κ_c was strongly dependent on volume. We therefore calculated the SF coupling at the value of κ_c appropriate to $L = 12a$ and then at a shifted value of κ. We present a comparison of the two cases in the Appendix. The shifted κ value gives a separate

TABLE II: Schrödinger functional couplings $1/g^2$ from this study.

β	κ_c	$1/g^2$			
		$L = 6a$	$L = 8a$	$L = 12a$	$L = 16a$
3.0	0.12682	0.5846(27)	0.5771(26)	0.5708(37)	0.5690(66)
2.5	0.1276	0.4417(27)	0.4378(25)	0.4273(34)	0.4268(50)
2.453	0.12766	0.4284(24)	–	0.4178(50)	–
2.445	0.12769	0.4305(27)	0.4170(37)	–	–
2.0	0.12967	0.2966(24)	0.2912(23)	0.2870(29)	0.2934(37)
1.985	0.12279	0.2912(24)	–	0.2801(48)	–
1.97	0.12991	0.2852(24)	0.2833(32)	–	–
1.75	0.13216	0.2165(24)	0.2164(21)	0.2122(29)	0.2157(34)
1.5	0.13617	0.1281(24)	0.1263(19)	0.1350(24)	0.1287(34)
1.4	0.13824	0.0655(29)	0.0790(21)	0.0950(27)	0.1035(34)

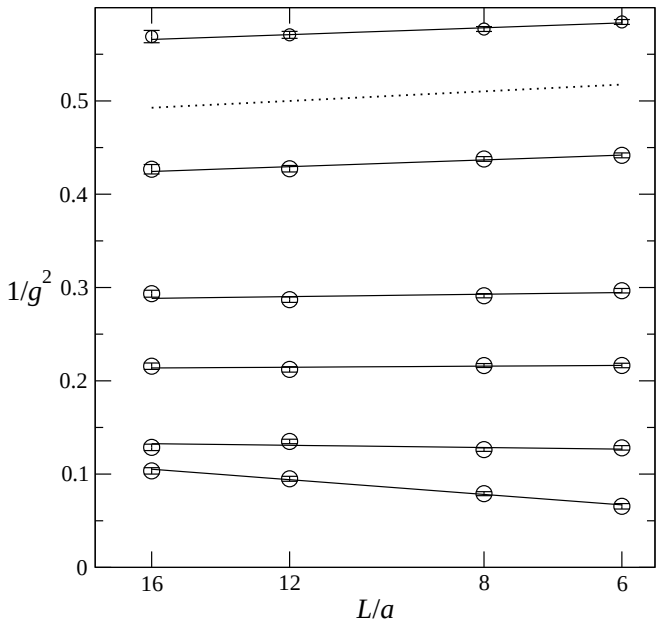

FIG. 5: SF coupling $1/g^2$ *vs.* L/a (plotted on a logarithmic scale) for the four volumes studied, at (from the top) $\beta = 3.0$, 2.5, 2.0, 1.75, 1.5, and 1.4. The lines through the data points are fits to the data at each β of the form $1/g^2(L) = a + b\log(L/a)$. The dotted line has the slope $2b_1/(16\pi^2)$ as given by the lowest-order beta function, Eq. (3).

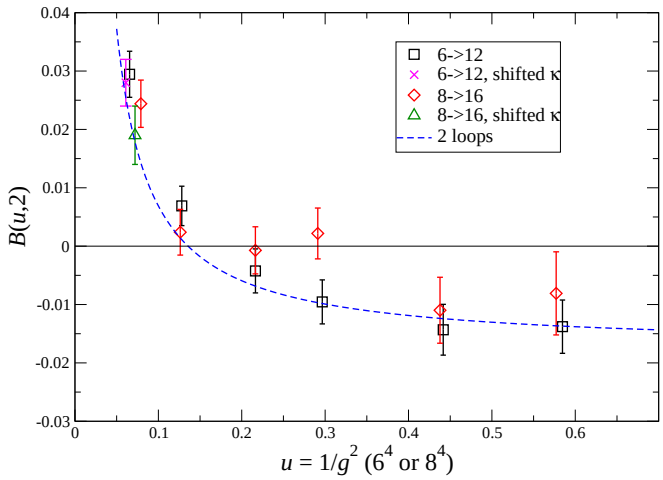

FIG. 6: Discrete beta function, Eq. (10), for scale factor $s = 2$ as a function of $1/g^2$ measured on the smaller lattice. Two values of L are shown for the smaller lattice, $L = 6$ and 8. The pairs of points correspond to calculations carried out at (right to left) $\beta = 3.0$, 2.5, 2.0, 1.75, 1.5, and 1.4, as shown in Fig. 5, plus points calculated at a shifted κ value at $\beta = 1.4$. The dashed line is the two-loop result. The shifted κ value is discussed in the Appendix.

determination of the DBF at $\beta = 1.4$, which is included in Fig. 6. One sees that the shift in κ leads to a change in the DBF that is less than the statistical error bar.

B. Finding g_* and estimating systematic error

As can be seen from Fig. 5, the spread of values of $1/g^2$ for different volumes at fixed bare coupling β is typically much smaller than the difference between values obtained at different β's. This motivates us to analyze the data in two stages. In the first stage, the data set at each β is treated as an independent fitting problem. The outcome is the value of the DBF at some reference value of $1/g^2$ reachable at that β. In the second stage, the DBF's from all β's are combined to obtain an estimate of g_*, the location of the IRFP. The variety of fits studied gives us a handle on the systematic error in g_*.

The data plotted in Fig. 5 are evidently linear in $\log(L/a)$ for fixed β. To study deviations from linearity we try fitting four different functions to $u \equiv 1/g^2(L)$:

$$u = a + b\log x, \tag{25a}$$
$$u = a + b\log x + c(\log x)^2, \tag{25b}$$
$$u = a + b\log x + c/x, \tag{25c}$$
$$u = a + b\log x + c/x^2. \tag{25d}$$

In these formulas, $x = L/8a$. The simplest fit, Eq. (25a), assumes linearity in $\log(L/a)$ and no discretization errors. The results of this fit at each bare coupling were plotted in Fig. 5. In Eq. (25b) we have added the next term from Eq. (17), reflecting subleading continuum running. In the last two fit functions we include instead a term that accounts for discretization errors. In Eq. (25c) we assume that the leading lattice artifacts are linear in a/L, whereas in Eq. (25b) they are assumed to be quadratic.

In the continuum limit, $a/L \to 0$, fits (25c) and (25d) both reduce to the simplest fit, Eq. (25a). The fit parameter a is thus interpreted as $1/g^2(L = 8a)$, while b is the estimate $R(g^2)$ for the beta function $\tilde{\beta}(1/g^2)$ at the same L. The parameters a and b have a similar interpretation for fit (25b) as well. In particular, since $\tilde{\beta}$ for $1/g^2(L = 8a)$ is $\partial u/\partial \log s$ evaluated at $s = 1$, this is again b.

We plot the fit parameter b, which gives the beta function, versus a, the inverse coupling, for each fit type in Fig. 7. The squares show results of fits using all four volumes, $L/a = 6$, 8, 12, 16. These fits have one degree of freedom, except for the simplest fit (25a) which has two degrees of freedom. We have included in panel (a) another fit to Eq. (25a) where only the three largest volumes ($L/a = 8$, 12, 16) are kept. This fit has one degree of freedom.

For almost all beta values, all of these fits produce χ^2/dof near unity; the exception is $\beta = 1.5$, where all fits give $\chi^2 \simeq 6$. The five fit types give results that are consistent with each other as well as with the two-loop beta function. We remark that all fits have good χ^2/dof at the strongest bare coupling, $\beta = 1.4$, leaving no doubt that the beta function has crossed zero.

Our next task is the determination of g_*, the value of the running coupling where the DBF vanishes. For each fit type, we can locate the zero by a linear fit to the points in its figure. In all cases, we get good χ^2 after dropping the points at the smallest ($\beta = 1.4$) and largest ($\beta = 3.0$) couplings. The final results are shown in Table III. One observes that all the results are mutually consistent.

The differences among the estimates quoted in Table III for $1/g_*^2$ reflect our systematic uncertainties, to which we now turn. Unlike in QCD, where all sources of systematic error are well under control, in the case of a (nearly) conformal theory the systematic error is poorly understood. Indeed, an important conclusion from Fig. 7 is that our data do not allow us to sort out discretization errors from subleading continuum corrections. With this in mind, we estimate the systematic error by keeping a subset of the five fit types that represents both options.

First, we obviously keep the simplest, linear fit (25a) on all four volumes. To account for the possibility of continuum corrections, we include fit (25b).

It remains to select a fit that represents the possible discretization errors. Here we face a difficulty. As can be seen in Fig. 7 and in Table III, fits (25c) and (25d), which both include a term for lattice artifacts, give significantly larger error bars than the other fits. This shows that our data do not resolve $\log x$ from $1/x^2$ (and, even more so, from $1/x$). We stress that our clover action with the nHYP links generally shows much smaller discretization errors than the simple Wilson action. Nonetheless, since we keep the clover coefficient at its tree-level value of 1, some residual linear dependence on a/L could survive.

Luckily, we have yet another fit type that is sensitive to the discretization errors and, at the same time, produces much tighter uncertainties in g_*. This is the simple fit (25a) in which we drop the smallest volume, $L = 6a$. Since the smallest volume necessarily contains the largest discretization errors, dropping it must give us a result that is closer to the continuum limit. The advantage of dropping the smallest volume in the linear fit over fits (25c) and (25d) is that there is no need to postulate anything about the concrete form of the discretization errors; in particular, we do not have to assume anything about the relative size of a/L and $(a/L)^2$ errors.

Disregarding fits (25c) and (25d) while keeping the other three, we finally conclude that

$$\frac{1}{g_*^2} = 0.20(4)(3), \tag{26}$$

where the first error is statistical and the second is systematic, representing the spread of the mean values of the three selected fit types. It follows that

$$g_*^2 = 5.0^{+2.7}_{-1.3}\ , \tag{27}$$

where we have combined the systematic and statistical errors linearly.[2]

The derivative of the beta function at the fixed point is a universal quantity. In our linear fits, reported in Table III, this is just the fit parameter B . We conclude

$$\left.\frac{d\tilde{\beta}}{du}\right|_{u=1/g_*^2} = -0.08(3). \tag{28}$$

This time the error is entirely statistical. The three fit types we have kept produce essentially the same result, so the systematic error is negligible. This translates into an exponent

$$y_g = \left.\frac{d\beta(g^2)}{dg^2}\right|_{g_*^2} = -\frac{1}{2}B = 0.040(15). \tag{29}$$

[2] Examination of our graphs shows that most of the systematic error is due to one data point for $1/g^2$, namely that at $\beta = 2.0$ for $L = 16a$. This is responsible for the high point in the $8 \to 16$ DBF plotted in Fig. 6 at $u \simeq 0.3$.

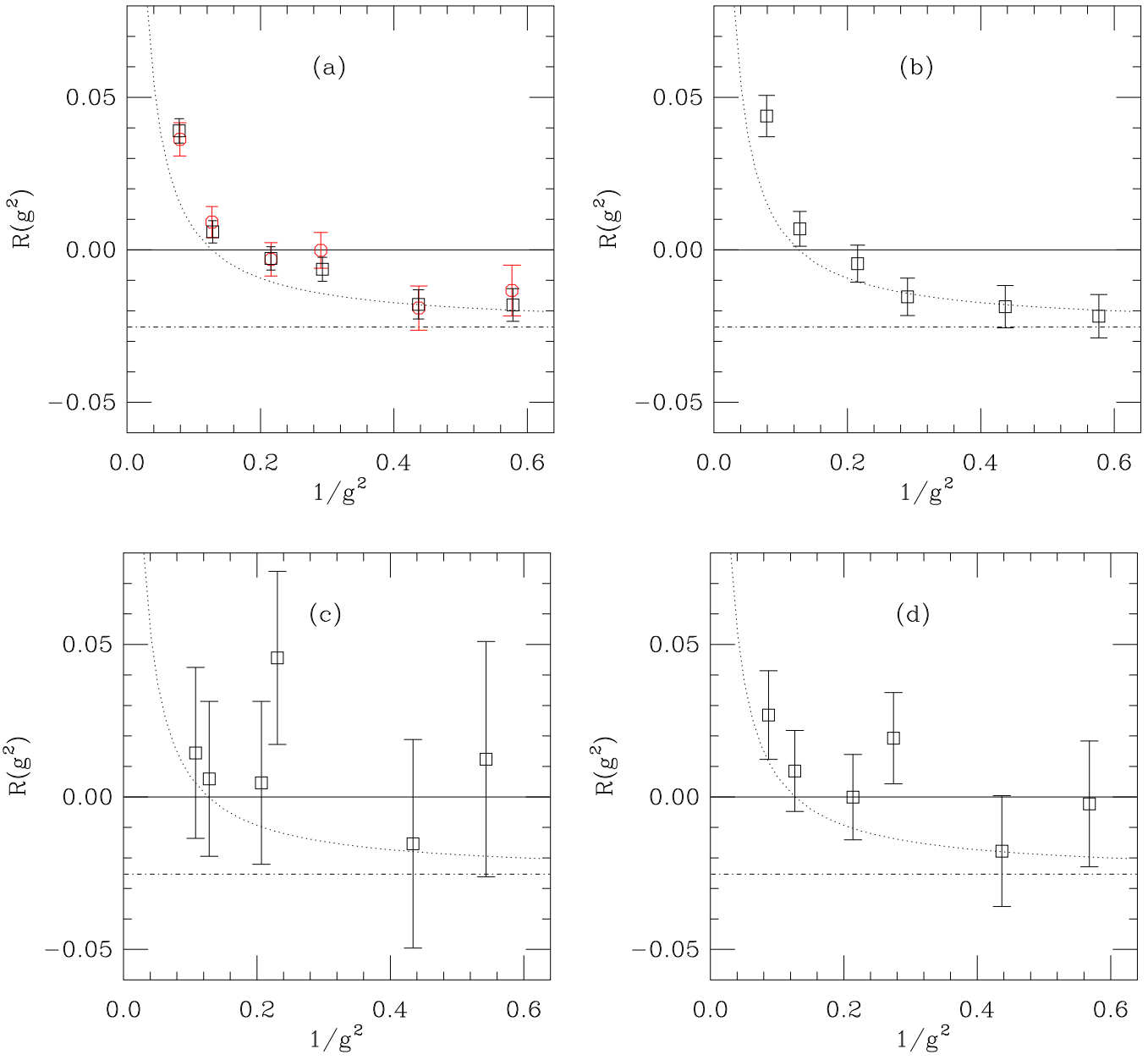

FIG. 7: Estimate $R(g^2)$ for the beta function $\tilde{\beta}(1/g^2)$ as extracted from the fits listed in Eq. (25). Each panel shows results of a different fit, as described more fully in the text: (a) Squares show fits to $a + b\log x$ using all four volumes; circles, using $L/a = 8$, 12, 16 only. (b) Fits to $a + b\log x + c(\log x)^2$. (c) Fits to $a + b\log x + c/x$. (d) Fits to $a + b\log x + c/x^2$. Plotted curves are the one-loop (dashed line) and two-loop (dotted line) beta functions.

TABLE III: Linear fits to the beta functions plotted in Fig. 7. Each beta function (resulting from the fitting procedure listed in the table) is a fit to $R(g^2) = A + B/g^2$, and the fit gives an estimate of the zero of R at g_*.

fit type giving beta function	A	B	$1/g_*^2$
(a) $a + b\log x$, all volumes	0.015(5)	−0.08(2)	0.20(3)
(a) $a + b\log x$, $L/a = 8$, 12, 16	0.019(7)	−0.08(3)	0.23(4)
(b) $a + b\log x + c(\log x)^2$	0.015(8)	−0.09(3)	0.17(4)
(c) $a + b\log x + c/x$	0.027(34)	−0.07(14)	0.40(41)
(d) $a + b\log x + c/x^2$	0.020(18)	−0.07(7)	0.31(13)

The positive sign indicates infrared irrelevancy of the gauge coupling.

C. Attempt to disentangle continuum running from lattice artifacts

Here we describe an attempt at a more traditional SF analysis, as described in Sec. II. As we have seen above, data taken at the same value of bare parameters, but at several values of L, will show a combination of true running and lattice artifacts. In principle, these effects can be separated: One adjusts the bare parameters in the simulation to match the SF coupling on two different-sized small lattices, and then increases the lattice sizes by the same scale factor s. A comparison of the DBF's obtained will show only lattice artifacts. This differs from our plot of the DBF for $s = 2$, Fig. 6, in that here we calculate $B(u, s)$ for fixed $u = 1/g^2$ with two different lattice spacings; in the plot we kept (β, κ) fixed, and hence the lattice spacing, between lattices with $L = 6a$ and $L = 8a$. It basically amounts to using lattice data at several couplings as a substitute for our fitting functions Eq. 25c or 25d.

We attempted such a match near two values of the bare coupling, $\beta = 2.0$ and 2.5. In Figs. 8 and 9, we calculate $B(u, 2)$ using $L = 8a$ and $16a$ at one bare parameter value β, and then use $L' = 6a'$ and $12a'$ at β'; the relation between β and β' is $u(L' = 6a', \beta') = u(L = 8a, \beta)$. We may then declare that $L' = L$ in physical units. We can also do the same exercise for $s = 4/3$ by starting with $L = 12a$ and $16a$ at β, matching to $L' = 6a'$ and $8a'$ at β'. The data for $1/g^2$ are shown in Fig. 8. It is apparent that matching the couplings, for example $u(L' = 6a', \beta')$ and $u(L = 8a, \beta)$, can only be accomplished within large error bars.

Fig. 9 shows the rescaled DBF $R(u, s)$ for scale factors $s = 4/3$ and 2. We plot R against $(a/L)^2$, and attempt to fit the data to a linear dependence in $(a/L)^2$. We can do it separately for each value of s, or, following the discussion in Sec. II, we can fit the rescaled DBF to a common line. The results of those fits are shown in the two figures. The fits of all the data give $\chi^2 = 0.4$ and 3.2 for two degrees of freedom at $\beta = 2.0$ and 2.5, respectively.

At $\beta = 2.5$, or $1/g^2 \simeq 0.42$, the continuum-extrapolated rescaled DBF $R(u, s)$ is 0.013(27) for $s = 4/3$, $-0.008(22)$ for $s = 2$, and 0.002(17) for the combined fit. The two loop result is -0.018, and our numerical result is consistent with it.

At $\beta = 2.0$, or $1/g^2 \simeq 0.27$, the continuum-extrapolated $R(u, s)$ is 0.031(22) for $s = 4/3$, 0.027(17) for $s = 2$, and 0.024(14) for the combined fit. This is 1.7σ away from zero. The two-loop result is -0.014, about 2σ away. The fits with many L's using Eqs. (25c)–(25d), which include *ansätze* for discretization errors, also produced a positive DBF with a large uncertainty at $\beta = 2.0$. The SF coupling is right on the edge of the value we quote in Eq. (26) for $1/g_*^2$ from our analysis of many couplings.

Notice that the analysis in this subsection underestimates the error in the DBF since we have not included the uncertainty in β' that arises from matching the SF couplings. To make a definitive determination of g_*^2 using the extrapolation method would require repeating it at many couplings with significantly better statistics. We conclude that this method is no better than fits to Eqs. (25c)–(25d). We have already argued that the other fits, Eqs. (25a)–(25b), give more reliable results.

TABLE IV: Values of Z_P, the pseudoscalar renormalization constant

β	κ_c	Z_P			
		$L = 6a$	$L = 8a$	$L = 12a$	$L = 16a$
3.0	0.12682	0.511(1)	0.490(1)	0.462(2)	0.441(2)
2.5	0.1276	0.484(1)	0.456(1)	0.423(1)	0.402(1)
2.0	0.12967	0.427(1)	0.394(1)	0.354(1)	0.332(1)
1.75	0.13216	0.373(1)	0.338(1)	0.301(2)	0.277(1)
1.5	0.13617	0.293(1)	0.261(1)	0.227(1)	0.203(1)
1.4	0.13824	0.250(3)	0.219(2)	0.188(1)	0.173(2)

V. MASS ANOMALOUS DIMENSION

Finally we turn to the mass anomalous dimension γ_m. Our analysis will parallel that of Sec. IV B with the difference that $\log Z_P(L)$ replaces $1/g^2(L)$.

Our data for $Z_P(L)$ are shown in Table IV and plotted in Fig. 10. The lines represent fits of the form of Eq. (24) to the data at each bare parameter value. The nearly straight-line behavior of the data is indicative of a slowly running coupling.

Fig. 11 shows the values of γ_m extracted using Eqs. (21) and (23) from pairs of lattices with scale factor $s = 2$. We have plotted the data as a function of the SF coupling g^2 measured on the smaller volume. There does not seem to be a great deal of difference between results from the two pairs, meaning that there is not much of a shift with lattice spacing. The rightmost points are from the strongest coupling, $\beta = 1.4$. As is clear in our various determinations of the DBF, the SF coupling does run significantly at this value of β. Note again that the $L = 6a$ coupling is larger than the $L = 8a$ coupling, indicative of the positive DBF.

The main feature of Fig. 11 is that the measured anomalous dimension γ_m at first follows closely the one-loop curve, but beyond $g^2 \simeq 4$ it flattens out.

As we did for the running coupling, we can fit $\log Z_P(L)$ to various functional forms. Again we begin with the simple linear behavior of Eq. (24); we proceed to add corrections with the aim of testing whether deviations reflect continuum corrections or lattice artifacts. We use the same fit functions, given in Eq. (25), with the change that u in these equations now stands

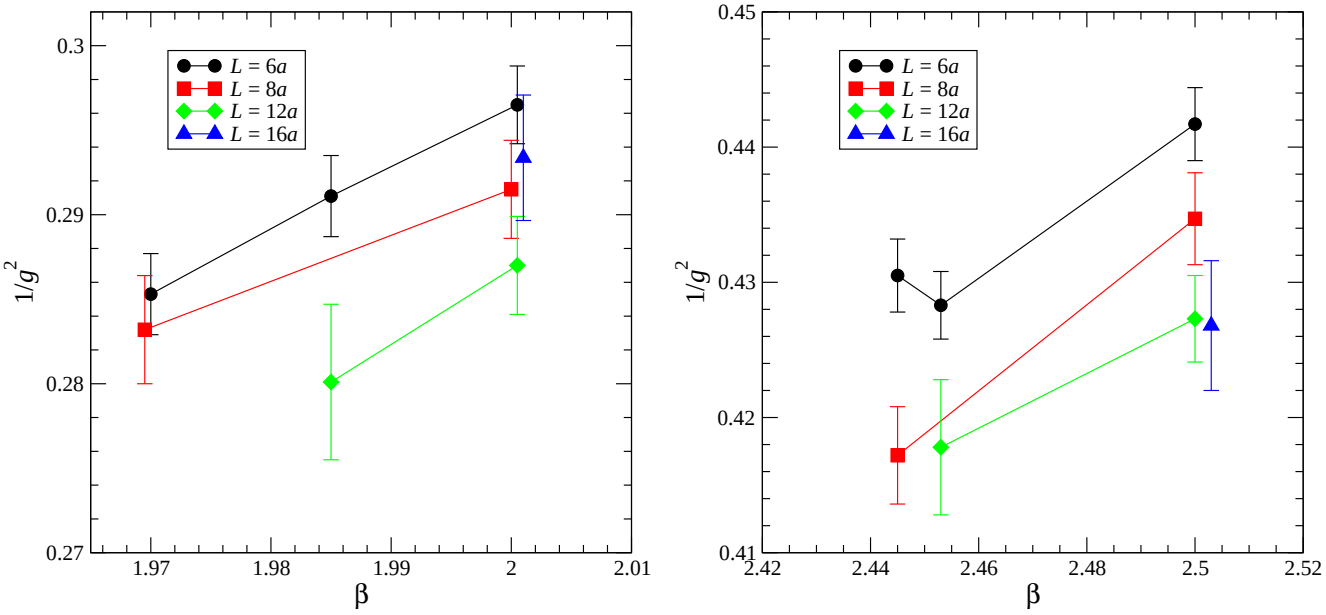

FIG. 8: $1/g^2$ near $\beta = 2.0$ (left) and $\beta = 2.5$ (right). Points at $\beta = 2.0$ and $\beta = 2.5$ are slightly displaced for clarity.

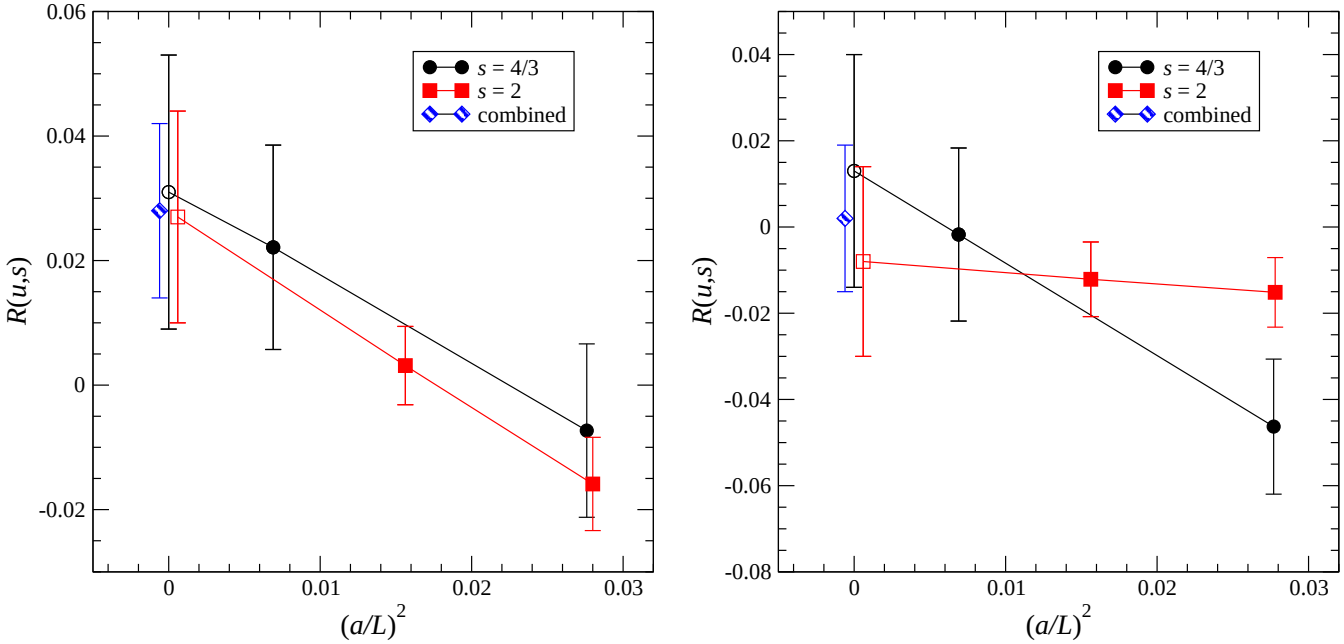

FIG. 9: Discrete beta functions near $\beta = 2.0$ (left) and $\beta = 2.5$ (right), where the smaller lattices' g^2 values are matched by slightly varying the bare parameters. The points near $(a/L)^2 = 0$ are the results of fits, described in the text: the circle is the extrapolation of $R(u, 4/3)$, the square is the extrapolation of $R(u, 2)$, and the diamond is a fit to all four points. Some points have been displaced slightly for clarity.

for $\log Z_P(L)$. The reasoning that led to the identification of the fit parameter b with $R(g^2)$ in Sec. IV B now leads to its identification with $-\gamma_m(g^2)$. The results are shown in Fig. 12. In all cases we plot γ_m as a function of $g^2(L = 8a)$, where the latter was obtained from the parallel fit type in Sec. IV B.

Our data for Z_p are far more precise than the data for $1/g^2$ given above. This is reflected in the much smaller error bars in Fig. 12 compared to Fig. 7. At the same time, this leads to rather high values of χ^2/dof (in the range 3–4) in the linear fits (24), whether we use three

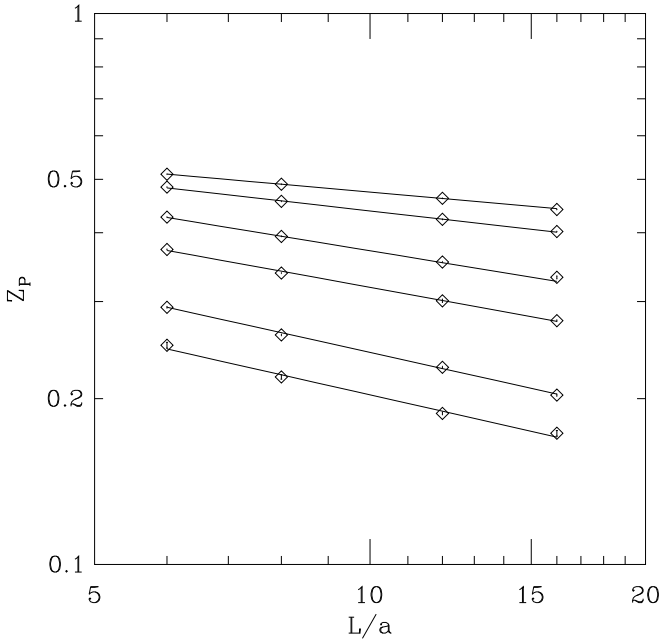

FIG. 10: Pseudoscalar renormalization constant Z_P. From the top, data are from $\beta = 3.0$, 2.5, 2.0, 1.75, 1.5 and 1.4. Lines are fits to $\log Z_P(L) = -\gamma_m \log(L/a) + \text{const}$ for each β.

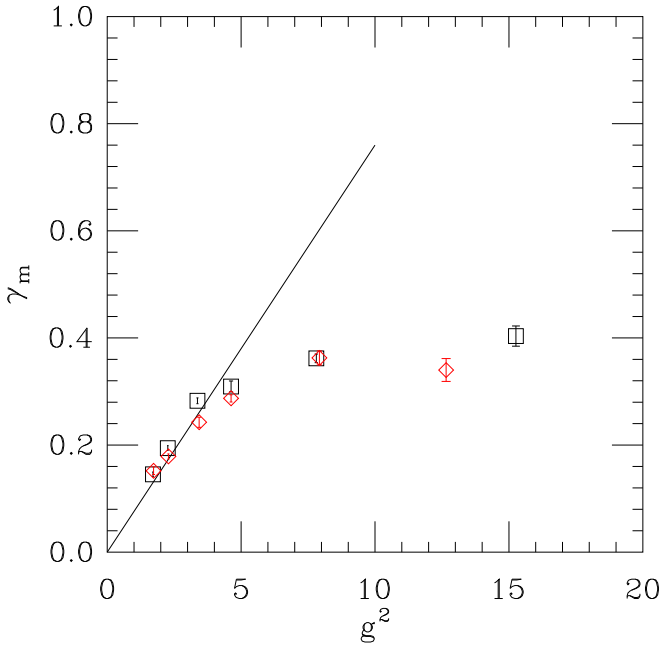

FIG. 11: Anomalous dimension γ_m calculated from $\sigma_P(v, s = 2)$ using Eq. (23) from pairs of lattices: $L/a = 6 \to 12$ (squares) and $L/a = 8 \to 16$ (diamonds). It is plotted as a function of the SF coupling g^2 on the smaller lattice size. Bare couplings range from $\beta = 3$ on the left to 1.4 on the right, as in Fig. 10. The line is the lowest-order perturbative result.

or four volumes. The χ^2 is good for the other three fits, again excepting $\beta = 1.5$ which gives $\chi^2/\text{dof} \simeq 6$.

Finally we estimate $\gamma_m(g_*)$, the mass anomalous dimension at the IRFP. The uncertainty in $\gamma_m(g_*)$ must reflect the uncertainties in the determination of g_* itself. In Fig. 13 we have plotted again our results for the linear fit to all four volumes. The horizontal bar at the top of the figure indicates our result for g_*^2, Eq. (27). We see that the right and left ends of the error bar almost coincide with the points corresponding to $\beta = 2.0$ (on the weak-coupling side) and $\beta = 1.5$ (on the strong-coupling side). This observation renders unnecessary any interpolation of the curve. In view of the monotonicity of $\gamma_m(g)$, we simply take the values of γ_m at these two couplings to mark off the uncertainty of $\gamma_m(g_*)$, concluding that

$$\gamma_m(g_*) = 0.31(6). \tag{30}$$

Roughly 5/6 of the error comes from the uncertainty in g_*. The small statistical and systematic errors of γ_m itself are responsible for the rest. Based on the same reasoning as in Sec. IV B, we took the spread of values obtained using the two linear fits [panel (a) of Fig. 12] and fit (25b) [panel (b)] as a measure of the systematic uncertainty in γ_m.

Fig. 13 also shows a comparison of our data to those of Bursa *et al.* [20], where we have applied to their data the linear fit (24). (Their published graphs include an additional large systematic uncertainty.) Our data lie slightly below theirs.

VI. DISCUSSION

Our simulations show that SU(2) gauge theory coupled to two flavors of adjoint fermions lies inside the conformal window. Using Schrödinger functional techniques, we have determined its IRFP and measured two exponents, the mass anomalous dimension γ_m and the exponent y_g of the (irrelevant) gauge coupling. Both are small.

Because the massless theory is conformal, not confining, it is not a candidate for a technicolor theory. Even if the theory were to be deformed in a way that destroys the IRFP, the small anomalous dimension would spell trouble for its application as a technicolor theory.

We are aware of several estimates of g_* and $\gamma_m(g_*)$ in the literature. The two-loop zero of the beta function occurs at $g_*^2 = 7.9$ which is right on the edge of our quoted range. Our central value is at weaker coupling, $g_*^2 = 5.0$.

The location of the IRFP is scheme dependent, of course. The previous lattice study with the best data, which also used the SF coupling to find a fixed point, is that of Hietanen *et al.* [17]. Their published analysis combines data from all L's and bare parameter values into a single fitting function. They quote fitted values of g_*^2 in the range 2.0–3.2, or $1/g_*^2$ in the range 0.3–0.5. We are in mild disagreement with their results. Their

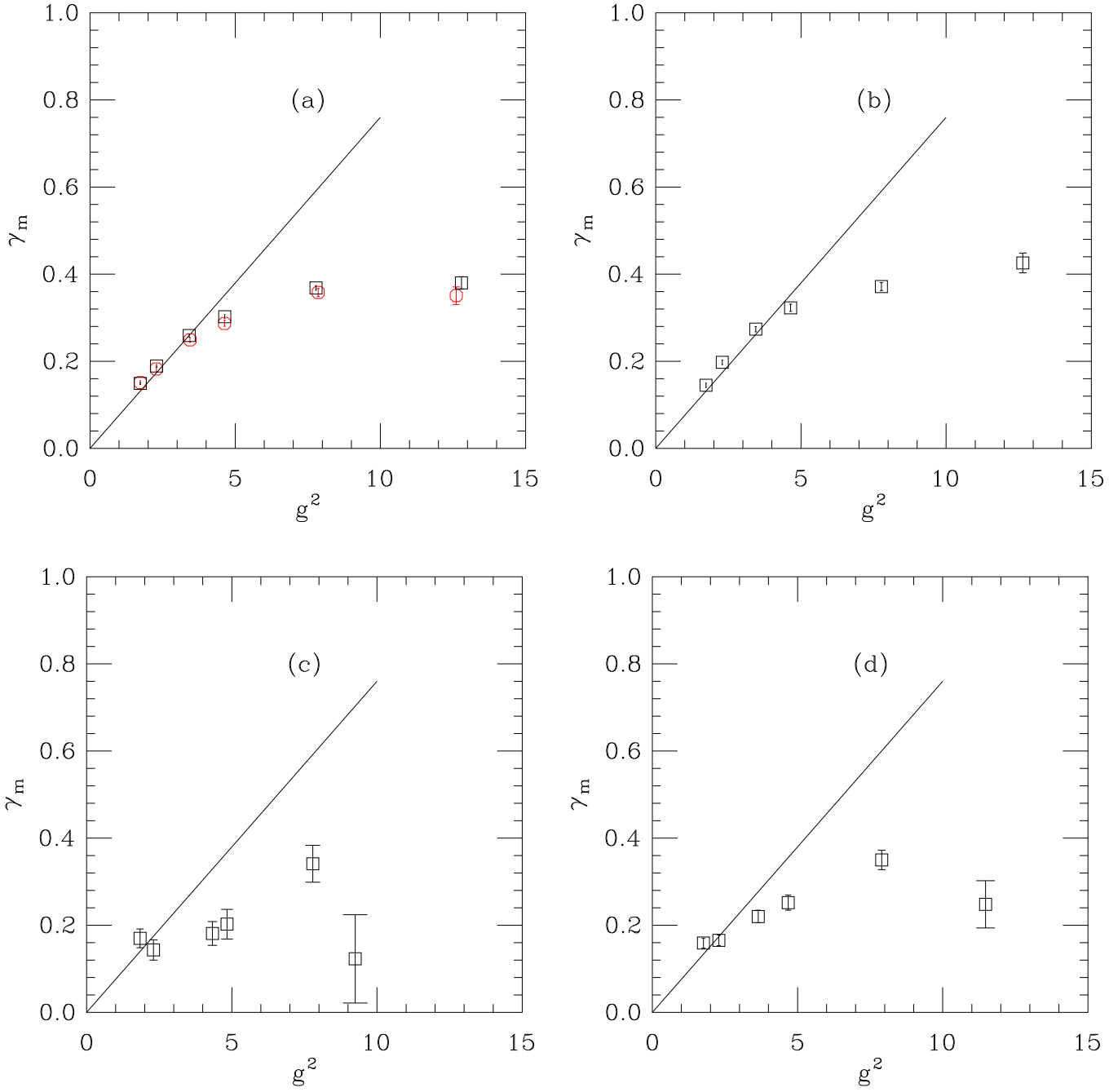

FIG. 12: γ_m from fits of $\log Z_p$ plotted as a function of $g^2(L = 8a)$: (a) Squares show fits to $a - \gamma_m \log x$, where $x = L/8a$, using all four volumes; circles, using $L/a = 8$, 12, 16 only. (b) Fits to $a - \gamma_m \log x + c(\log x)^2$. (c) Fits to $a - \gamma_m \log x + c/x$. (d) Fits to $a - \gamma_m \log x + c/x^2$. The line in each case is the one-loop result.

lattice action uses unimproved Wilson fermions with no clover term, and hence is susceptible to $O(a)$ discretization errors. The line of first order transitions also extends farther into weaker coupling in their case; they have no data below $1/g^2 = 0.22$.

As seen in Fig. 13, our results for $\gamma_m(g^2)$ agree with the earlier determination of Bursa *et al.* [20], where we overlap in couplings. We also agree with the MCRG result of Catterall *et al.* [23], $\gamma_m(g_*) = 0.49(13)$, given its larger uncertainty. Del Debbio *et al.* [21, 22] use the scaling of spectral observables with fermion mass to compute γ_m at $g^2 \simeq 3$, finding small values [0.05–0.20 and 0.22(6) respectively]. These results also lie on the lowest-order perturbative curve.

We find that $\gamma_m(g^2)$ deviates from the lowest-order perturbative formula for $g^2 \gtrsim 4$. As we saw for SU(3)

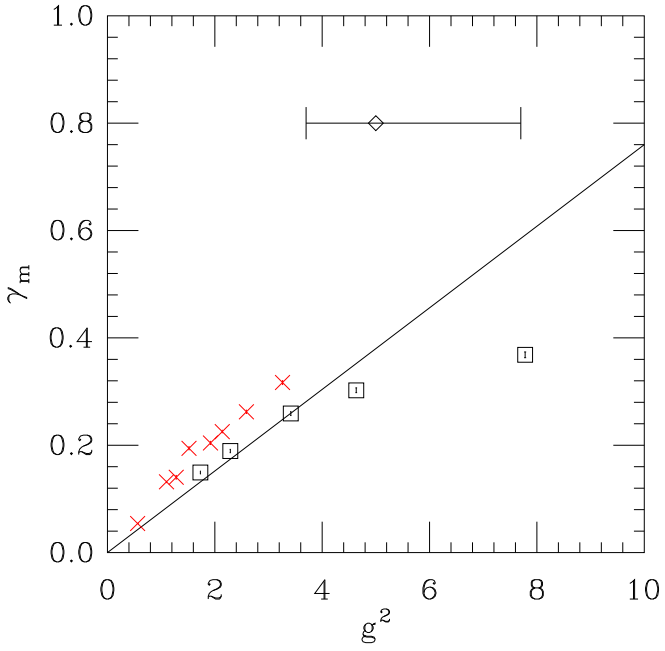

FIG. 13: Mass anomalous dimension $\gamma_m(g^2)$ from the linear fit (24), which are the squares in Fig. 12(a). The horizontal bar at the top marks our result (27) for g_*^2. The crosses are the data of Bursa, et al. [20], analyzed with the same linear fit. Again the diagonal line is the perturbative result.

with sextet fermions, the numerical results lie below the curve.

Now let us consider analytic predictions for $\gamma_m(g_*)$. Ryttov and Shrock [42] have an extensive tabulation of perturbative results up to four loops in the $\overline{MS}$ scheme (see also [43]). Recall that only anomalous dimensions measured at fixed points are scheme-independent. Perturbative predictions of course depend on the order of perturbation theory. They tabulate $\gamma_m(g_*) = 0.820$, 0.543, 0.500 for two, three, and four loops. They also give a prediction based on solving a Schwinger–Dyson equation, $\gamma_m(g_*) = 0.653$. The Ryttov–Sannino all-orders beta function [44] gives $\gamma_m(g_*) = 0.75$. Pica and Sannino offer another all-orders beta function [45] which gives $\gamma_m(g_*) = 0.46$. All these numbers are too high to agree with our result.

There is an extensive literature attempting to relate the location of the bottom of the conformal window to a large value for γ_m (see [44, 46] and references therein). Our results indicate that models using the SU(2) gauge group and adjoint fermions are not relevant to that literature: the parameter space accessible to exploration is too granular. Our γ_m is small. One might want to decrease N_f in the hope that γ_m would grow as one approaches the bottom of the conformal window. This is clearly not possible here: The $N_f = 1$ theory has $b_2 > 0$ and is probably confining.

Finally, we point out that the use of an improved action, which smooth the gauge field fluctuations as seen by the fermions, made this project feasible. It shifts the location of the strong-coupling transition deeper into strong coupling than could be achieved with the simple Wilson action, allowing us access to the strong coupling side of the IRFP.

Acknowledgments

B. S. and Y. S. thank the University of Colorado for hospitality. This work was supported in part by the Israel Science Foundation under grant no. 423/09 and by the U. S. Department of Energy. Computations were done on clusters at the University of Colorado and Tel Aviv University. Additional computations were done on facilities of the USQCD Collaboration at Fermilab, which are funded by the Office of Science of the U. S. Department of Energy. Our computer code is based on the publicly available package of the MILC collaboration [47]. The code for hypercubic smearing was adapted from a program written by A. Hasenfratz, R. Hoffmann and S. Schaefer [48].

Appendix: Determining κ_c

For each value of the bare coupling β we determined κ_c by demanding $m_q = 0$ for $L = 12a$. We calculated m_q in a series of short runs over a range of κ's, eventually confirming $m_q = 0$ in a run of several hundred trajectories. When we used this value of κ_c in the much longer runs that yielded the SF coupling g^2, the error bar on m_q naturally shrank and thus the final result for m_q is always a little bit off zero.

We used the same values of (β, κ_c) for different lattice volumes, so as to keep the lattice spacing fixed for the SF calculation. In the weak-coupling region, the volume dependence of κ_c is weak, as seen in Fig. 14. In particular, m_q on the 16^4 lattice is small enough that we can say that $m_q \simeq 0$ in the infinite-volume limit. This is not the case, however, at stronger couplings (Fig. 15). Of particular concern is the large value of m_q for the strongest coupling, $\beta = 1.4$, on the largest lattice, $L = 16a$; the value $\kappa_c = 0.13284$ is perfectly adequate for $L = 12a$ but not for $L = 16a$ (see Table V).

In principle, one could fix κ_c by demanding that $m_q \to 0$ in the infinite volume limit, which can be done by fitting to finite-volume results at various values of κ. As is clear from Fig. 15, the finite-lattice corrections to m_q are proportional to $(a/L)^2$, as may be expected for the clover action. This procedure would involve lengthy calculations, however, since the error bars shown in the figure are only attainable with the statistics of a full SF simulation. We decided instead to check on the sensitivity of our results to a shift in κ of the order that might be required by this procedure.

Table V and Fig. 15 show the values of $m_q a$ calculated at the nominal $\kappa_c = 0.13824$ and at a shifted value $\kappa =$

TABLE V: AWI masses $m_q a$ at $\beta = 1.4$ for the two κ values considered.

β	κ	$m_q a$			
		$L = 6a$	$L = 8a$	$L = 12a$	$L = 16a$
1.4	0.13824($\equiv \kappa_c$)	0.092(2)	0.035(1)	0.0013(4)	-0.0092(3)
1.4	0.1381	0.109(3)	0.053(2)	0.0128(6)	0.0014(3)

TABLE VI: Schrödinger functional couplings $1/g^2$ at $\beta = 1.4$ for the two κ values.

β	κ	$1/g^2$			
		$L = 6a$	$L = 8a$	$L = 12a$	$L = 16a$
1.4	0.13824($\equiv \kappa_c$)	0.0655(29)	0.0790(21)	0.0950(27)	0.1035(34)
1.4	0.1381	0.0610(21)	0.0722(24)	0.0891(34)	0.0926(34)

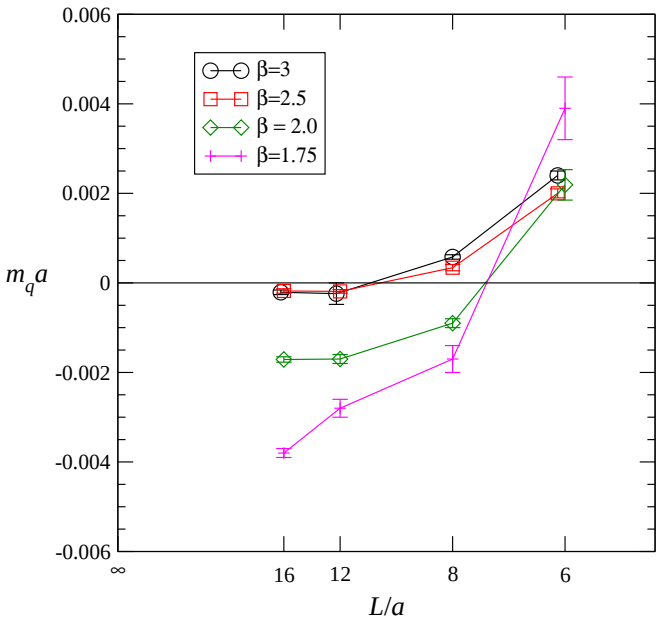

FIG. 14: Volume dependence of the AWI mass m_q at fixed β, where κ was fixed by a preliminary determination of $m_q = 0$ on the 12^4 lattice.

0.1381 that gives a small value of $m_q a$ for the largest lattice $L = 16a$. Table VI lists the SF couplings $1/g^2$ for all four volumes at both values of κ. While the shift in κ does induce a significant and systematic shift in $1/g^2$, the change in the DBF is much smaller than the statistical error, as is seen in Fig. 6. A similar result obtains for Z_P (Table VII); the ratios σ_P are unaffected and thus the estimate of γ_m is unaffected as well. We conclude that our results are insensitive to such shifts in κ, even at the strongest coupling studied. Note that we have not made use of any of the data at $\beta = 1.4$ in determining g_* or $\gamma_m(g_*)$.

[1] G. T. Fleming, "Strong interactions for the LHC," PoS **LATTICE2008**, 021 (2008) [arXiv:0812.2035 [hep-lat]].

[2] E. Pallante, "Strongly and slightly flavored gauge theories," PoS **LAT2009**, 015 (2009) [arXiv:0912.5188 [hep-lat]].

[3] L. Del Debbio, "The conformal window on the lattice," PoS **LATTICE2010**, 004 (2010).

[4] T. DeGrand, "Lattice studies of QCD-like theories with many fermionic degrees of freedom," arXiv:1010.4741 [hep-lat].

[5] K. Rummukainen, "QCD-like technicolor on the lattice," arXiv:1101.5875 [hep-lat].

[6] For a review see C. T. Hill and E. H. Simmons, "Strong dynamics and electroweak symmetry breaking," Phys. Rept. **381**, 235 (2003) [Erratum-ibid. **390**, 553 (2004)] [arXiv:hep-ph/0203079];

[7] W. E. Caswell, "Asymptotic behavior of nonabelian gauge theories to two loop order," Phys. Rev. Lett. **33**, 244 (1974).

[8] T. Banks and A. Zaks, "On the phase structure of vector-like gauge theories with massless fermions," Nucl. Phys. B **196**, 189 (1982).

[9] T. DeGrand, "Finite-size scaling tests for SU(3) lattice gauge theory with color sextet fermions," Phys. Rev. D

TABLE VII: Pseudoscalar renormalization constant Z_P at $\beta = 1.4$ for the two κ values.

β	κ	Z_P			
		$L = 6a$	$L = 8a$	$L = 12a$	$L = 16a$
1.4	0.13824($\equiv \kappa_c$)	0.250(3)	0.219(2)	0.188(1)	0.173(2)
1.4	0.1381	0.237(2)	0.2105(13)	0.182(3)	0.1645(15)

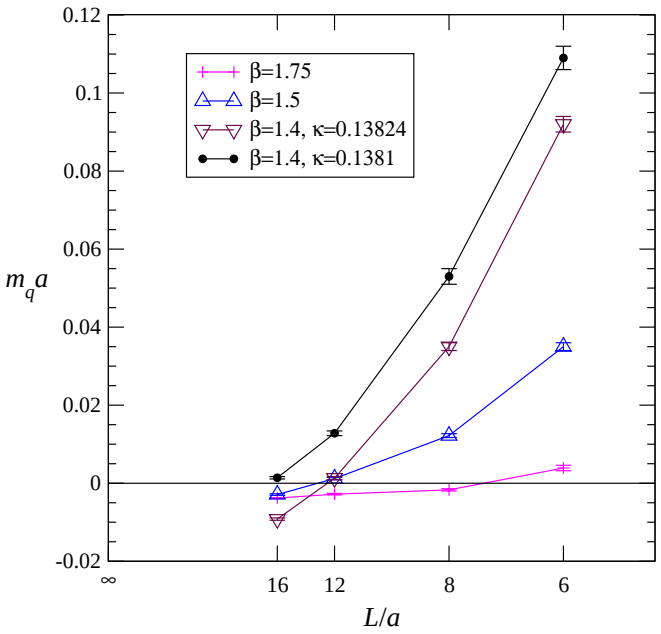

FIG. 15: Same as Fig. 14, but at stronger bare couplings β. The data for $\beta = 1.75$ are the same as in Fig. 14, to show the change in vertical scale.

80, 114507 (2009) [arXiv:0910.3072 [hep-lat]].

[10] L. Del Debbio and R. Zwicky, "Hyperscaling relations in mass-deformed conformal gauge theories," Phys. Rev. D **82**, 014502 (2010) [arXiv:1005.2371 [hep-ph]].

[11] F. Sannino and K. Tuominen, "Orientifold theory dynamics and symmetry breaking," Phys. Rev. D **71**, 051901 (2005) [arXiv:hep-ph/0405209].

[12] D. D. Dietrich and F. Sannino, "Conformal window of SU(N) gauge theories with fermions in higher dimensional representations," Phys. Rev. D **75**, 085018 (2007) [arXiv:hep-ph/0611341].

[13] S. Catterall and F. Sannino, "Minimal walking on the lattice," Phys. Rev. D **76**, 034504 (2007) [arXiv:0705.1664 [hep-lat]].

[14] L. Del Debbio, A. Patella and C. Pica, "Higher representations on the lattice: numerical simulations. SU(2) with adjoint fermions," Phys. Rev. D **81**, 094503 (2010) [arXiv:0805.2058 [hep-lat]].

[15] S. Catterall, J. Giedt, F. Sannino and J. Schneible, "Phase diagram of SU(2) with 2 flavors of dynamical adjoint quarks," JHEP **0811**, 009 (2008) [arXiv:0807.0792 [hep-lat]].

[16] A. J. Hietanen, J. Rantaharju, K. Rummukainen and K. Tuominen, "Spectrum of SU(2) lattice gauge theory with two adjoint Dirac flavours," JHEP **0905**, 025 (2009) [arXiv:0812.1467 [hep-lat]].

[17] A. J. Hietanen, K. Rummukainen and K. Tuominen, "Evolution of the coupling constant in SU(2) lattice gauge theory with two adjoint fermions," Phys. Rev. D **80**, 094504 (2009) [arXiv:0904.0864 [hep-lat]].

[18] L. Del Debbio, B. Lucini, A. Patella, C. Pica and A. Rago, "Conformal vs confining scenario in SU(2) with adjoint fermions," Phys. Rev. D **80**, 074507 (2009) [arXiv:0907.3896 [hep-lat]].

[19] S. Catterall, J. Giedt, F. Sannino and J. Schneible, "Probes of nearly conformal behavior in lattice simulations of minimal walking technicolor," arXiv:0910.4387 [hep-lat].

[20] F. Bursa, L. Del Debbio, L. Keegan, C. Pica and T. Pickup, "Mass anomalous dimension in SU(2) with two adjoint fermions," Phys. Rev. D **81**, 014505 (2010) [arXiv:0910.4535 [hep-ph]].

[21] L. Del Debbio, B. Lucini, A. Patella, C. Pica and A. Rago, "Mesonic spectroscopy of Minimal Walking Technicolor," Phys. Rev. D **82**, 014509 (2010) [arXiv:1004.3197 [hep-lat]].

[22] L. Del Debbio, B. Lucini, A. Patella, C. Pica and A. Rago, "The infrared dynamics of Minimal Walking Technicolor," Phys. Rev. D **82**, 014510 (2010) [arXiv:1004.3206 [hep-lat]].

[23] S. Catterall, L. Del Debbio, J. Giedt and L. Keegan, "MCRG Minimal Walking Technicolor," PoS **LATTICE2010**, 057 (2010) [arXiv:1010.5909 [hep-ph]].

[24] A. Hasenfratz and F. Knechtli, "Flavor symmetry and the static potential with hypercubic blocking," Phys. Rev. D **64**, 034504 (2001) [arXiv:hep-lat/0103029].

[25] A. Hasenfratz, R. Hoffmann and S. Schaefer, "Hypercubic smeared links for dynamical fermions," JHEP **0705**, 029 (2007) [arXiv:hep-lat/0702028].

[26] T. DeGrand, Y. Shamir and B. Svetitsky, "Running coupling and mass anomalous dimension of SU(3) gauge theory with two flavors of symmetric-representation fermions," Phys. Rev. D **82**, 054503 (2010) [arXiv:1006.0707 [hep-lat]].

[27] B. Sheikholeslami and R. Wohlert, "Improved continuum limit lattice action for QCD with Wilson fermions," Nucl. Phys. B **259**, 572 (1985).

[28] S. Capitani, S. Dürr and C. Hoelbling, "Rationale for UV-filtered clover fermions," JHEP **0611**, 028 (2006) [arXiv:hep-lat/0607006].

[29] S. Dürr *et al.*, "Scaling study of dynamical smeared-link clover fermions," Phys. Rev. D **79**, 014501 (2009) [arXiv:0802.2706 [hep-lat]].

[30] Y. Shamir, B. Svetitsky and E. Yurkovsky, "Improvement via hypercubic smearing in triplet and sextet QCD," arXiv:1012.2819 [hep-lat].

[31] M. Hasenbusch, "Speeding up the Hybrid-Monte-Carlo algorithm for dynamical fermions," Phys. Lett. B **519**, 177 (2001) [arXiv:hep-lat/0107019].

[32] C. Urbach, K. Jansen, A. Shindler and U. Wenger, "HMC algorithm with multiple time scale integration and mass preconditioning," Comput. Phys. Commun. **174**, 87 (2006) [arXiv:hep-lat/0506011].

[33] T. Takaishi and P. de Forcrand, "Testing and tuning new symplectic integrators for hybrid Monte Carlo algorithm in lattice QCD," Phys. Rev. E **73**, 036706 (2006) [arXiv:hep-lat/0505020].

[34] M. Lüscher, R. Narayanan, P. Weisz and U. Wolff, "The Schrodinger functional: A renormalizable probe for non-Abelian gauge theories," Nucl. Phys. B **384**, 168 (1992) [arXiv:hep-lat/9207009].

[35] M. Lüscher, R. Sommer, P. Weisz and U. Wolff, "A precise determination of the running coupling in the SU(3) Yang–Mills theory," Nucl. Phys. B **413**, 481 (1994) [arXiv:hep-lat/9309005].

[36] S. Sint and R. Sommer, "The running coupling from the QCD Schrödinger functional: A one loop analysis," Nucl. Phys. B **465**, 71 (1996) [arXiv:hep-lat/9508012].

[37] K. Jansen and R. Sommer [ALPHA collaboration], "O(α) improvement of lattice QCD with two flavors of Wilson quarks," Nucl. Phys. B **530**, 185 (1998) [Erratum-*ibid.* B **643**, 517 (2002)] [arXiv:hep-lat/9803017].

[38] M. Della Morte *et al.* [ALPHA Collaboration], "Computation of the strong coupling in QCD with two dynamical flavours," Nucl. Phys. B **713**, 378 (2005) [arXiv:hep-lat/0411025].

[39] S. Sint and P. Weisz [ALPHA collaboration], "The running quark mass in the SF scheme and its two-loop anomalous dimension," Nucl. Phys. B **545**, 529 (1999) [arXiv:hep-lat/9808013].

[40] S. Capitani, M. Lüscher, R. Sommer and H. Wittig [ALPHA Collaboration], "Non-perturbative quark mass renormalization in quenched lattice QCD," Nucl. Phys. B **544**, 669 (1999) [arXiv:hep-lat/9810063].

[41] M. Della Morte *et al.* [ALPHA Collaboration], "Non-perturbative quark mass renormalization in two-flavor QCD," Nucl. Phys. B **729**, 117 (2005) [arXiv:hep-lat/0507035].

[42] T. A. Ryttov and R. Shrock, "Higher-loop corrections to the infrared evolution of a gauge theory with fermions," arXiv:1011.4542 [hep-ph].

[43] C. Pica and F. Sannino, "UV and IR zeros of gauge theories at the four loop order and beyond," [arXiv:1011.5917 [hep-ph]].

[44] T. A. Ryttov and F. Sannino, "Supersymmetry inspired QCD beta function," Phys. Rev. **D78**, 065001 (2008). [arXiv:0711.3745 [hep-th]].

[45] C. Pica and F. Sannino, "Beta Function and Anomalous Dimensions," arXiv:1011.3832 [hep-ph].

[46] D. B. Kaplan, J. W. Lee, D. T. Son and M. A. Stephanov, "Conformality Lost," Phys. Rev. D **80**, 125005 (2009) [arXiv:0905.4752 [hep-th]].

[47] `http://www.physics.utah.edu/~detar/milc/`

[48] A. Hasenfratz, R. Hoffmann and S. Schaefer, "Low energy chiral constants from epsilon-regime simulations with improved Wilson fermions," Phys. Rev. D **78**, 054511 (2008) [arXiv:0806.4586 [hep-lat]].